

Article

A Novel Humidification Technique Used in Water Desalination Systems Based on the Humidification–Dehumidification Process: Experimentally and Theoretically

Ahmed E. Tourab ^{1,2,*} , Ana María Blanco-Marigorta ³ , Aly M. Elharidi ¹ and María José Suárez-López ² 

¹ Arab Academy for Science and Technology and Maritime Transport, Mechanical Engineering Department, Alexandria 21611, Egypt; Alyelharidi@aast.edu

² EDZE (Energía), Campus de Viesques, Universidad de Oviedo, 33204 Gijón, Asturias, Spain; suarezlmaria@uniovi.es

³ Departamento de Ingeniería de Procesos, Edificio de Ingenierías-Tafira Baja, Universidad de Las Palmas de Gran Canaria, 35017 Las Palmas G.C., Spain; anamaria.blanco@ulpgc.es

* Correspondence: ahmedessam@aast.edu

Received: 9 May 2020; Accepted: 3 July 2020; Published: 12 August 2020



Abstract: In this paper, an experimental and theoretical investigation is performed on a novel water desalination system based on a humidification–dehumidification technique using a heat pump. An ultrasonic water atomizer is used in the humidification process in order to improve the humidification system. In addition to that, a new configuration is employed in the humidification process (hybrid atomization system), which combines the traditional spraying atomization system and the ultrasonic water atomizer. The new humidification system performance is investigated and compared with the spraying water atomizer system in terms of humidification effectiveness and freshwater productivity. The results show that the ultrasonic water atomizer has enhanced and improved humidification effectiveness, and consequently, the productivity of freshwater. The maximum humidification effectiveness and productivity achieved by the ultrasonic water atomizer are 94.9% and 4.9 kg/h, respectively, meaning an increase of 25.2% and 18.8%, compared to the traditional spraying atomization system. The hybrid system increases humidification effectiveness and productivity by 3.8% and 8.2%, respectively, in comparison with the stand-alone ultrasonic water atomizer. A cost analysis was also carried out in this paper in order to perform an economic comparison of different humidification processes (spraying, ultrasonic; and hybrid atomization systems). The minimum production cost of one liter of freshwater amounts to \$0.0311 with the spraying system, \$0.0251 with the ultrasonic system, and \$0.0250 with the hybrid atomization system. These results reveal the profitability of the new configuration.

Keywords: humidification-dehumidification; desalination; ultrasonic atomization; hybrid system

1. Introduction

Freshwater plays an important role in human life. However, it is not plentiful. Saline water is available in abundance and represents 97% of the water on the planet, with the remaining 3% being freshwater, but unfortunately, most of it is concealed at the two poles of the Earth and in mountain ice caps. Although beneficial freshwater also comprises ground and surface water, these sources represent only 30.4% of the total freshwater available [1]. According to the United Nations World Water Development Report [2], global water demand is increasing at a high rate. More than 2 billion

people live in high water risk countries. While the global average water stress is only 11%, 31 countries face water stress between 25% and 70%, and 22 countries are above 70% [2]. It is foreseen that, in order to cover these freshwater requirements, desalination techniques will play an important role in the short term.

Conventional desalination methods, including Multi-Stage Flash (MSF), Multi-Effect Evaporation (MEE), and Reverse Osmosis (RO), are valid for wide freshwater output ranges of 100–50,000 m³/day [3]. However, such methods are costly for the limited amounts of freshwater they produce, and they cannot be used in areas like islands and remote regions, where relatively low maintenance and energy resources are available. Humidification–Dehumidification Desalination (HDH) is a safe, promising desalination technology suitable for low-quality energy sources such as low-temperature solar or waste heat energies. This method has several advantages, such as the ability to operate with low-grade heat energy, constant pressure, and low running costs, making it suitable for producing freshwater in remote rural areas [4–8]. The HDH system concept consists of two steps: 1. A fluid (ambient air) goes through a duct where water is sprayed or sprinkled. In this way, the air becomes saturated (humidification process). 2. The water vapor held by the saturated fluid is condensed (dehumidification process); as a result, freshwater is produced.

Regarding the humidification process, in the literature, there are two methods commonly used. The first one uses a pad humidifier. It has a honeycomb structure where saline water is sprinkled and atomized. In the second one, the saline water is atomized using water sprayers.

With respect to the first method, there are several papers that have varied the material of the pad humidifier. Zamen et al. [9] evaluated the optimum number of stages in the HDH process, using a polypropylene packed bed humidifier. The two-stage process improved the specific energy usage, efficiency and daily output per collector area, and also the investment costs. This process was around 20% more efficient than the single-stage one. Kabeel and Said [10] experimentally studied a hybrid solar desalination system based on HDH. The pad humidifier consisted of PVC reaching rings. In this case, the maximum humidification efficiency was 98% at midday on a sunny day, and the maximum productivity was 45 L/day. Hamed et al. [11] mathematically and experimentally studied a solar water heated HDH desalination system. The humidification process was achieved using a pad humidifier made from Cellulose paper. The average freshwater productivity was 22 L/day. Other investigations have studied this process using a mechanical vapor compression heat pump (Gao et al. [12], Yuan et al. [13]), increasing the productivity up to 60 L/day. Finally, Xu [14] improved a water desalination system with a cellulose pad, using waste heat from the air-cooling condenser. They achieved a maximum humidification effectiveness of 65% and a productivity of 129 kg/day.

Regarding the second method, spray humidifiers, there are also several studies. Yanniotis and Xerodemas [15] experimentally investigated two types of air humidification spray and pad humidifiers under different operating conditions. They demonstrated that a water droplet eliminator is necessary in the spray humidifier. Kang et al. [16] assessed the performance of a multi-effect desalination system based on humidification-dehumidification. The main target was to make use of the latent heat of condensation and the residual heat in the brine and reuse it. The maximum GOR was 2.44 and the production of freshwater 72.6 kg/h. Hawlader et al. [17] experimentally studied an HDH system with a modified solar assisted heat pump. The trials showed that the higher the compressor work and the inlet water temperature, the higher the productivity. Hegazy et al. [18] experimentally investigated an HDH system with a heat pump. They analyzed different flow directions of the spray water and observed that the highest evaporation rate was achieved by the cross-flow spraying system. Later, El-Maghlany et al. [19] improved the desalination system of Hegazy et al. [18], increasing the productivity using a parallel spraying flow.

There are several papers investigating other methods for improving the humidification process. Elminshawy et al. [20] presented an experimental and analytical study on a solar HDH desalination system where two water heaters of 500 W and a sunray reflector were used in the humidification process. Gang et al. [21] sprayed warm water on porous balls in the humidification process and

achieved an increase of 67.44% when the sprayed water temperature was increased from 60 °C to 90 °C using the HDH principle. Two solar collectors were used to heat the air and water. The proposed system showed high humidification efficiency in the middle of the day, as the solar radiation was high in this period. Agouz and Abugderah [22] experimentally studied the air humidification process by passing air through saline water to generate an air column of bubbles inside the saline water. The experimental results indicated that the humidification efficiency and vapor content were mainly affected by saline water temperature, while the air temperature had a small effect. The maximum humidification efficiency achieved was 95% when the temperature of saline water was about 75 °C. Ghazal et al. [23] presented a nontraditional HDH system enabling a more compact design by swapping certain components of a traditional HDH desalination unit with a solar collector. Air passed through the water-filled solar collector into the humidifier as bubbles. It was observed that humidification via direct contact bubbling could be efficient in the solar HDH desalination system. In fact, heat and mass transfer between air and water could be improved by increasing the air/water contact surface by using inverted sieves to modify the air bubbles. Sieves have improved heat transfer by acting as solar absorbers, further improving air carrying capacity by increasing the air temperature.

Another technology that could be used for humidification purposes is ultrasonic atomization. It is used in many technological operations, including therapeutic nebulizers, surface coatings, and liquid fuel sprays [24]. For many years, ultrasonic atomization has been an area of interest, as spray consistency or fineness is an essential requirement. The liquid droplet disintegration during ultrasonic atomization is explained by a conjunction of two main hypotheses: the capillary wave and the cavitation hypotheses, as shown in Figure 1. Ultrasonic excitation produces capillary waves at the liquid–gas interface, which becomes volatile due to the pinch-off of droplets from the wave peaks. While the cavitation theory indicates that as the transducer ultrasonic waves spread through the liquid phase, during the sound wave rarefaction process, the local fluid pressure drops below the vapor pressure due to vapor bubbles forming. Such cavitation bubbles explode aggressively during the compression process and unleash hydraulic shocks, breaking the liquid–gas interface and leading to atomization. Despite being an already-known technology, and highly effective, it has seldom been used in HDH water desalination systems. Just Zhang et al. [25] used an ultrasonic water atomizer for HDH water desalination. The study assessed the effect of both water temperature and salinity on the rate of evaporation. Unfortunately, the authors did not evaluate the salinity of the produced water. Nevertheless, their experiments showed that ultrasonic atomization could improve the desalination process, especially humidification efficiency. They also recommended this new methodology for seawater desalination.

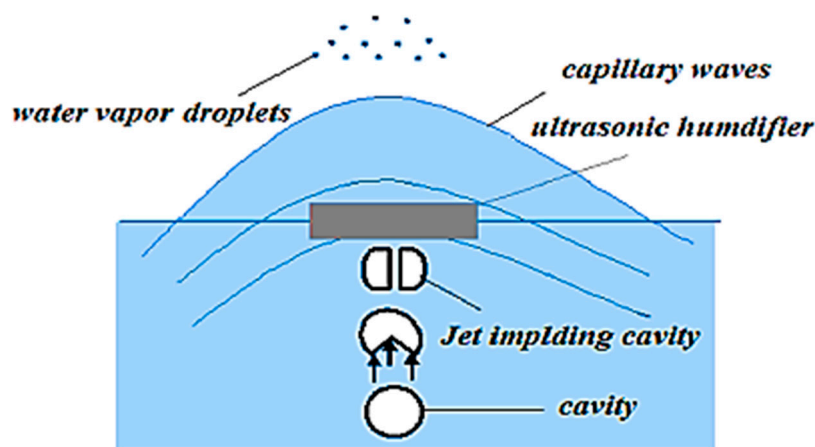


Figure 1. A simple schematic diagram shows the working principle of an ultrasonic atomizer.

According to the literature review, it was found that the humidification processes could and should be improved. Zhang et al. [25] pointed out that ultrasonic atomizer technology could be a good

option. However, the literature related to the use of this technology in HDH desalination processes is scarce. This new technology needs further research, especially in assessing the capabilities of this new technique in water atomization taking into account the effect of feed water salinity on freshwater production. In this paper, a novel study related to the usage of ultrasonic atomizer technology for water atomization in HDH desalination is performed. An experimental and theoretical investigation was carried out, and is presented in the following sections. The humidification effectiveness and the productivity of the new process were calculated and compared with the results provided by traditional spraying atomization. Moreover, the quality of freshwater production is investigated in both systems at different salinities and temperatures of the feed water. Additionally, a hybrid concept is presented here, combining the traditional and the ultrasonic atomizer to detect the maximum capability of this system.

2. Description of the Desalination System

The basic experimental desalination system was previously proposed by our research group El-Maghlany et al. [19]. The system is based on a humidification–dehumidification technique consisting of three main components: a humidifier, a dehumidifier, and a heat pump. A picture and a schematic diagram are shown in Figures 2 and 3, respectively. The heat pump is composed of five devices: an evaporator, a condenser, a compressor, a tree of capillary tubes, and a small heat exchanger located between the discharge line of the evaporator and the suction line of the heat pump compressor. The system configuration is based on an Open-air, Open-water cycle, and is air heated (AH). Air is withdrawn using a forced draft fan with two variable air dampers. As the air passes through the heat pump condenser, the air dry-bulb temperature increases. While the air crosses the heat pump condenser, the refrigerant is condensed, which consequently increases the air temperature. As the dry bulb temperature increases, the air becomes gluttonous to water.



Figure 2. Experimental setup of the desalination system.

Hot air gets humidified in the humidifier using two techniques. Firstly, a spray humidifier spraying saline water in parallel flow to the airflow. Secondly, by an ultrasonic atomizer generating a high-frequency sound wave. In the spray humidification step, a water eliminator is used to avoid the passage of any droplet of saline water to the other components of the system. After the humidification process, saturated air passes through a water-cooled heat exchanger (WCHE), simulating the effect of the weather conditions on saline water source temperature (three temperatures—15 °C, 20 °C, and 25 °C—were tested). The dehumidification process consists of two sections. The first is made up of the water-cooled heat exchanger, which improves the dehumidification process as it gets rid of some latent heat in the saturated air. In the other section, moist air passes through the heat pump evaporator; as a result, the heat content of moist air decreases, which is led in condensation of the water vapor, and freshwater is obtained. Finally, after the dehumidification process, the air is weeded out far from the working space in order to maintain the same operating conditions for all the experiments.

The experiments carried out using different saline water of TDS at 35 (Mediterranean Sea), 7, 6, 5, 4, 3, 2, 1, and 0.35 g/kg.

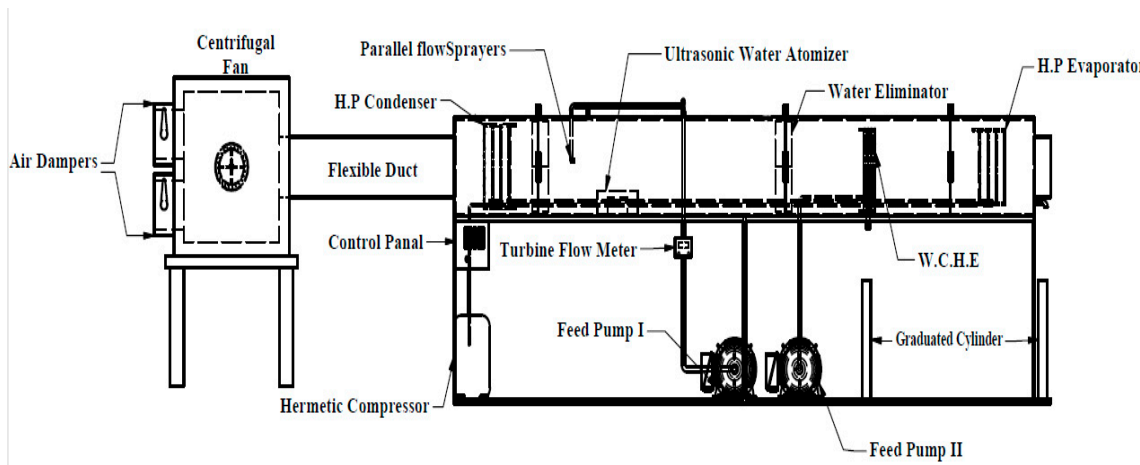


Figure 3. Schematic diagram of the components of the desalination system.

3. Experimental Configuration and Measurement Instruments

Experiments were carried out to determine the mass and heat transfer at each stage and to show the effect of the use of an ultrasonic water atomizer (novel humidification system) in the humidification process. Two sets of experiments were carried out: one of them using only an ultrasonic water atomizer in the humidification process, and the other using a hybrid system of humidification methods consisting of the direct spraying of water by means of an ultrasonic water atomizer. In this second scenario, the ultrasonic water atomizer gets the saline water from the drain of the spraying system.

3.1. Experimental Setup

Figure 4 shows a schematic of the process.

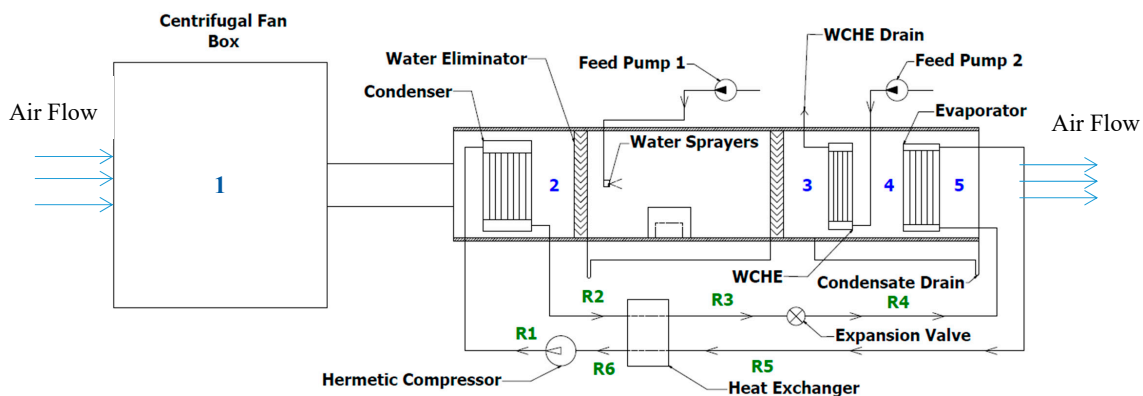


Figure 4. Schematic of the humidification–dehumidification desalination process.

The first section (1) of the experiment consists of a blower fan placed inside a cubic shape box $900 \times 900 \times 900 \text{ mm}^3$. The box walls are made of 20 mm thick galvanized steel. A filter is placed in the suction face wall to prevent the hanged particles from reaching the fan. A wooden plate with two air gates is used to plug the entrance face and to provide control of the fan’s airflow rate. After that, in section (2), the heat pump compressor of a maximum power of 2.35 kW is turned on, and the heat pump starts to work. As the heat pump runs, the forced draft air passes through a condenser which is fitted inside a $530 \times 400 \text{ mm}^2$ cross-sectional area and 510 mm long duct made of 20-mm-thick insulated galvanized steel. The airflow undertakes a sensible heating process using

the heat rejected from the condenser's heat pump. The condenser consists of a 195 aluminum finned copper tube with 3/8 inches in outer diameter. The fins are rectangular plates with a $530 \times 400 \text{ mm}^2$ cross-sectional area. The humidification process is achieved in section (3) either by spraying saline water in parallel flow to the airflow or by using an ultrasonic water atomizer. The humidifier duct made of 20-mm-thick insulated galvanized steel with a $530 \times 400 \text{ mm}^2$ cross-sectional area and which is 1500 mm long. It is also provided with two removable glass-windows to view what is happening inside. The spray humidifier has two identical sprayers formed by four holes of 0.5 mm diameter each, with an inlet spinning cavitation to each hole increasing the water atomization. The maximum saline water flow rate is 132 kg/h, using a 0.37 kW water pump. The ultrasonic water atomizer (the novel humidification method) consists of 10 probe heads fixed on a 304 stainless steel shell to resist corrosion and a waterproof transformer of a 0.36 kW input power as shown in Figure 5. The direct current voltage and the current of the ultrasonic water atomizer were adjusted to be 48 V and 5 A, respectively, producing an oscillation frequency of 1.7 MHz in order to produce 5 kg/h of atomized water. At the end of this section, there is a water droplet eliminator to remove any water droplets. The dehumidification process is divided into two sections, (4) and (5). In section (4), a water-cooled heat exchanger, made of 3/8-inch copper tubes with 169 aluminum rectangular fins, is used. It consists of 12 rows and 4 columns with two inlets: the first one on the first two columns and the other one on the second two columns. The WCHE is fitted in a duct of $530 \times 400 \text{ mm}^2$ cross-sectional area and 1000 mm long. A flow rate of 270 kg/h is fed to the WCHE using a 0.37 kW water pump. In the last section, the air passes through the heat pump evaporator, consisting of 177 aluminum rectangular fins, where the heat is removed from the moist air and the water vapor is condensed.



Figure 5. Ultrasonic water atomizer used in the experiments.

3.2. Data Collection

During the experiments, and to assess the desalination unit performance, several parameters including airflow rate changes, inlet and outlet air temperatures, inlet and outlet cooling water temperatures, relative air humidity before and after each process, and system productivity were measured.

The productivity of the unit is considered under steady-state conditions. It is found that the unit requires 20 to 30 min for the steady-state operating condition to be satisfied. In this state, all the parameters measured by the instruments are recorded. As we already detailed in Section 3.1, the process includes air heating (a heat pump condenser), humidification (water sprayers or an ultrasonic water atomizer), and two dehumidification processes (water cold heat exchanger and a heat pump evaporator). The dry-bulb temperature and the relative humidity are measured using a calibrated sensor (DHT 22) before and after each process. The sprayed water flow rate is measured using an electronic turbine digital flow meter. Air mass flow rate is estimated by calculating the average air velocity, which is measured using a vane anemometer. The measured air velocity distribution across the circular cross-sectional area of the flexible duct, connected between the fan and the heat pump condenser duct, is integrated to give the mass flow rate accurately. Each experimental data point

is the average of five individual measurements. The technical specifications of the instrumentation used in the experiments are illustrated in Table 1.

Table 1. Technical specifications of the instruments used in the experimental set-up.

Measuring Instrument	Accuracy	Range
Testo 416 Telescopic van-anemometer	±0.2 m/s	0.6 to 40 m/s
Hanna Instruments HI 9564	3% RH	20 to 95% RH
Thermo-hygrometer	±0.5 °C	0 to 60 °C
K24 Electronic turbine Digital flow meter	±1.0%	6 to 120 L/min
Digital Temperature & Humidity Sensor Module (DHT22)	5% RH	0–100%
Waterproof temperature sensor	±0.5 °C	−40 to 80 °C
Digital Clamp Meter HC-440D	±1.5%	0 to 400 Ampere
	±1.2%	0 to 750 Volt
E-Type Thermocouple	±1.7 °C	−270 to 870 °C

3.3. Error Analysis

Depending on the precision of each measuring instrument, uncertainty was calculated using Kline and McClintock propositions [26]. The highest uncertainties calculated for the freshwater produced, the electric power consumed, water to air mass flow rate ratios, and specific productivity are 3.2%, 2.7%, 8.7%, and 5.9%, respectively.

4. Theoretical Model

Both energy and mass transfer balances of different elements of the systems are described in terms of unit size, operational conditions, and weather conditions. The steady-state approach for simulating the system assumes that there is no energy contained in each component's building materials, thus ignoring the heat capacity of the materials.

To evaluate and investigate the performance of various parameters, such as air temperature, water temperature after each process, and productivity of the system, a mathematical model is developed. It solves energy balance equations for the heat pump condenser, humidifier, water-cooled heat exchanger and heat pump evaporator, where the previous parameters were studied under different conditions.

4.1. Heat Pump Condenser

The energy balance in the heat pump condenser, taking into consideration the steady-state condition, can be described as shown in Equation (1):

$$\dot{Q}_{in,C} - \dot{Q}_{out,C} - \dot{Q}_{L,C} = 0 \quad (1)$$

where \dot{Q} is the rate of heat transfer. This heat is introduced to the heat pump condenser via compressed refrigerant \dot{m}_R , and specific enthalpy $h_{R,1}$. Moreover, there is heat that gets into the condenser from the ambient air of $h_{a,1}$. Therefore,

$$\dot{Q}_{in,C} = \dot{m}_R \times h_{R,1} + \dot{m}_a \times h_{a,1} \quad (2)$$

Due to the heat exchange between the hot refrigerant and ambient, air and refrigerant flows leave the heat pump condenser with an enthalpy of $h_{a,2}$ and $h_{R,2}$, where air becomes dry and greedy to hold water vapor, while the refrigerant is condensed by losing its heat to the air.

$$\dot{Q}_{out,C} = \dot{m}_R \times h_{R,2} + \dot{m}_a \times h_{a,2} \quad (3)$$

The heat loss of the heat pump condenser to the atmosphere is determined using an analytical approach, assuming an average temperature, $T_{avg,C}$, around the ambient temperature T_{amb} .

$$\dot{Q}_{L,C} = U_{L,C} \times A_C \times (T_{avg,C} - T_{amb}) \quad (4)$$

where $T_{avg,C}$ is the average temperature between the refrigerant outlet temperature and the surrounding ambient temperature, so it can be written as follows:

$$T_{avg,C} = \frac{T_{R,2} + T_{amb}}{2} \quad (5)$$

Then, substituting Equations (2)–(4) into Equation (1), Equation (6) is obtained:

$$\dot{m}_a \times (h_{a,1} - h_{a,2}) + \dot{m}_R \times (h_{R,1} - h_{R,2}) + U_{L,C} \times A_C \times (T_{avg,C} - T_{amb}) = 0 \quad (6)$$

where $U_{L,C}$ is the overall heat transfer coefficient and A_C is the outside surface area of the heat pump condenser.

The overall heat transfer coefficient in the condenser represents the sum of thermal resistance per unit area. It can be defined as:

$$U_{L,C} = \left[\frac{1}{h_{conv,out} \times \eta_{overall,fin}} + \frac{1}{\left[A_{out} \times \frac{\ln\left(\frac{r_{out}}{r_{in}}\right)}{2\pi k_{fin} L_C} \right]} + \frac{A_{out}}{h_{conv,in} \times A_{in}} \right]^{-1} \quad (7)$$

while the overall fin efficiency can be calculated using Equation (8):

$$\eta_{overall,fin} = 1 - \frac{A_{fin}}{A_C \times (1 - \eta_{fin})} \quad (8)$$

The fin efficiency in the condenser can be defined as:

$$\eta_{fin} = \frac{\tanh(mm \times L_C)}{mm \times L_C} \quad (9)$$

where mm is:

$$mm = \sqrt{\frac{h_{conv,out} \times P_C}{k_{fin} \times A_{fin}}} \quad (10)$$

In the heat pump condenser, the outside heat transfer coefficient of the tubes as presented in [27] is:

$$h_{conv,out} = \frac{0.29 k_{air}}{d_{out,C}} \times Re_a^{0.633} \times Pr_a^{\frac{1}{3}} \times F_{HDH}^{-0.17} \quad (11)$$

$$F_{HDH} = \frac{SS_{fin}}{SS_{smooth}} \quad (12)$$

where F_{HDH} is the ratio of the surface area of the tube with fin per unit of length of the tube to the surface area without fin [28]:

$$SS_{fin} = \frac{A_C}{L_C} \quad (13)$$

$$SS_{smooth} = \frac{A_{C,without,fin}}{L_C} \quad (14)$$

4.2. Humidifier

In the humidification process, the flow of spraying saline water is in parallel with the airflow according to our previous results (El-Maghlany et al. [19]), which indicated that the highest humidification effectiveness and productivity were obtained with the parallel spraying system. Therefore, the model of the humidification process is based on a parallel-flow heat exchange between the sprayed saline water and the airflow. Furthermore, in the case of using an ultrasonic water atomizer, it produces water vapor, which is also flowing in the same direction as the airflow.

The energy balance in the humidification section, taking into consideration the steady-state condition, is presented in the following subsections.

4.2.1. Spraying System

$$\dot{Q}_{in,H} - \dot{Q}_{out,H} - \dot{Q}_{L,H} = 0 \quad (15)$$

where energy inlet to the humidifier is

$$\dot{Q}_{in,H} = \dot{m}_a \times h_{a,2} + \dot{m}_{sw} \times c_{p,sw} \times T_{sw,in} \quad (16)$$

while energy outlet from the humidifier is

$$\dot{Q}_{out,H} = \dot{m}_a \times h_{a,3} + \dot{m}_{sw} \times c_{p,sw} \times T_{sw,out} \quad (17)$$

Finally, energy loss at humidifier is

$$\dot{Q}_{L,H} = U_{L,H} \times A_H \times (T_{avg,H} - T_{amb}) \quad (18)$$

Then, by substituting Equations (16)–(18) into Equation (15), the total system energy balance for a humidifier is found as follows:

$$\dot{m}_a \times (h_{a,2} - h_{a,3}) + \dot{m}_{sw} \times c_{p,sw} (T_{sw,in} - T_{sw,out}) + U_{L,H} \times A_H \times (T_{avg,H} - T_{amb}) = 0 \quad (19)$$

Air enthalpy is determined by air temperature and humidity as reported in [11]:

$$h_a = (c_{p,a} + (c_{p,v} \times \omega_a)) \times T_a + (h_{fg} \times \omega_a) \quad (20)$$

The effectiveness of the humidification process can be calculated using Equation (21) for a parallel flow arrangement [27]:

$$\varepsilon_H = \frac{1 - \exp[-NTU \times (1 + C_r)]}{1 + C_r} = \frac{\dot{Q}_{actual}}{\dot{Q}_{max}} \quad (21)$$

where C_r is the heat capacity ratio of air/water (minimum-to-maximum) streams, NTU is the number of transfer units, \dot{Q}_{actual} is the actual heat transferred, and \dot{Q}_{max} is the maximum possible heat that could be transferred.

$$NTU_H = \frac{U_{L,H} \times A_H}{C_{min}} \quad (22)$$

$$\dot{Q}_{max} = C_{min} \times (h_{max} - h_{min}) \quad (23)$$

where C_{min} is the minimum heat capacity of the air or water stream. It is related to the mass flow rate ratio of the HDH cycle, as presented by Sharqawy et al. [29]

$$C_{min} = \min \left\{ \frac{M_{ratio} \times C_{sw}}{C_a}, \frac{C_a}{M_{ratio} \times C_{sw}} \right\} \quad (24)$$

The mass transfer rate in the humidifier as presented in [11]:

$$\dot{m}_a \times (h_{a,3} - h_{a,2}) = e \times k \times a \times V_H \times \left[\frac{(h_{sw,in} - h_{a,2}) - (h_{sw,out} - h_{a,3})}{\ln \left[\frac{(h_{sw,in} - h_{a,2})}{(h_{sw,out} - h_{a,3})} \right]} \right] \quad (25)$$

where (k) is the mass transfer coefficient, (a) is the humidifier substratum specific area, and (V_H) is the humidifier volume. While (e) is, the correction factor due to the direction of the flow is equal to one because the flow here is parallel.

4.2.2. Ultrasonic Atomizer

In the case of using an ultrasonic atomizer, the atomized feed water output is assumed to be saturated vapor, where the enthalpy of the output water vapor, $h_{vap,out}$ is determined by both the inlet feed water temperature and the atmospheric pressure. According to this, the model of the ultrasonic atomizer is the same as the model of the spraying system except for the following Equation (26):

$$\dot{Q}_{out,H} = \dot{m}_a \times h_{a,3} + \dot{m}_{vap} \times h_{vap,out} \quad (26)$$

4.2.3. Hybrid System

The hybrid system combines the spraying and the ultrasonic atomization techniques. To determine the properties of the humidified air after the combined process, the mixture of the humidified air from the spraying system and the water vapor produced by the ultrasonic atomizer is considered. The enthalpy of the mixture can be finally calculated using Equation (27):

$$h_{mixture} = (h_{a,3} \text{ (spraying)} \times \dot{m}_a + h_{a,3} \text{ (ultrasonic)} \times \dot{m}_{vap}) / (\dot{m}_a + \dot{m}_{vap}) \quad (27)$$

4.3. Dehumidifier

The dehumidification process is divided into two successive sections so that in the first section, the moist air passes through a water-cooled heat exchanger (WCHE). Meanwhile, in the second, moist air passes through the heat pump evaporator.

4.3.1. Water-Cooled Heat Exchanger

Similarly, the energy balance in the WCHE can be written as follows:

$$\dot{Q}_{in,WCHE} - \dot{Q}_{out,WCHE} - \dot{Q}_{L,WCHE} = 0 \quad (28)$$

where energy inlet to the WCHE is

$$\dot{Q}_{in,WCHE} = \dot{m}_a \times h_{a,3} + \dot{m}_{cw} \times c_{p,cw} \times T_{cw,in} \quad (29)$$

while energy outlet from the WCHE is

$$\dot{Q}_{out,WCHE} = \dot{m}_a \times h_{a,A} + \dot{m}_{cw} c_{p,cw} \times T_{cw,out} \quad (30)$$

Finally, energy loss at WCHE is

$$\dot{Q}_{L,WCHE} = U_{L,WCHE} \times A_{WCHE} \times (T_{avg,WCHE} - T_{amb}) \quad (31)$$

Then, by substituting Equations (29)–(31) into Equation (28), the total system energy balance for WCHE is obtained as follows:

$$\dot{m}_a \times (h_{a,3} - h_{a,4}) + \dot{m}_{cw} \times c_{p,cw} (T_{cw,in} - T_{cw,out}) + U_{L,WCHE} \times A_{WCHE} \times (T_{avg,WCHE} - T_{amb}) = 0 \quad (32)$$

The effectiveness of the WCHE can be calculated using Equation (33), where the flow between cooling water and moist air is a crossflow arrangement [27]:

$$\varepsilon_{WCHE} = \left(\frac{1}{C_r} \right) \times [1 - \exp\{-C_r \times (1 - \exp(-NTU))\}] \quad (33)$$

4.3.2. Heat Pump Evaporator

Continuing the dehumidification process, energy balance is also performed in the second stage of the dehumidification process and written as follows:

$$\dot{Q}_{in,E} - \dot{Q}_{out,E} - \dot{Q}_{L,E} = 0 \quad (34)$$

where energy inlet to the evaporator is

$$\dot{Q}_{in,E} = \dot{m}_a \times h_{a,4} + \dot{m}_R \times h_{R,4} \quad (35)$$

while energy outlet from the evaporator is

$$\dot{Q}_{out,E} = \dot{m}_a \times h_{a,5} + \dot{m}_R \times h_{R,5} \quad (36)$$

Finally, energy loss at the evaporator is

$$\dot{Q}_{L,E} = U_{L,E} \times A_E \times (T_{avg,E} - T_{amb}) \quad (37)$$

Then, by substituting Equations (35)–(37) into Equation (34), the total system energy balance for the evaporator is found as follows:

$$m_a \times (h_{a,4} - h_{a,5}) + m_R \times (h_{R,4} - h_{R,5}) + U_{L,E} \times A_E \times (T_{avg,E} - T_{amb}) = 0 \quad (38)$$

The distillate flow rate is estimated from a mass balance, taking into account the difference in water content among air inlet and outlet from the dehumidification process, where distilled water is accumulated. This distillation rate is defined as presented by [19]:

$$m_{FW} = m_a \times (\omega_{a,3} - \omega_{a,5}) \quad (39)$$

4.4. Solution Technique

The mathematical modeling for the heat pump condenser, humidifier, and dehumidifier is solved using MATLAB 2015. The following parameters are considered as shown:

Flow rates: \dot{m}_a , \dot{m}_R , \dot{m}_{sw} , \dot{m}_{vap} , and \dot{m}_{cw}

Fluid properties: $c_{p,a}$, $c_{p,w}$, $c_{p,v}$, $c_{p,R}$, and h_{fg}

Dimensions (external and internal): Heat pump condenser, humidifier, water-cooled heat exchanger, and heat pump evaporator.

T_{amb} is considered constant.

The performance of the heat pump is constant.

To assess the desalination process performance, specific productivity is used and calculated using Equation (40), which defines the amount of freshwater produced per unit of energy (kWh),

$$\text{Specific productivity} = \frac{\dot{m}_{Fw} \times 3600}{\text{Energy consumption / hour}} \quad (40)$$

where *energy consumption* is calculated by getting the electric *energy consumption* for each component using electricity, such as a heat pump compressor, centrifugal fan, saline water feed pump, and the ultrasonic water atomizer. Therefore, electric power consumption can be written as follows:

$$\dot{W}_{elec} = V \times I \quad (41)$$

5. Results and Discussion

The proposed theoretical model is related to the spraying atomization method, which was already validated by our previous work [19]. The main results are shown in Figure 6, in terms of the productivity of the desalination unit. A mean deviation of only 0.168 was observed between the productivity calculated by the physical model and by the experimental data. In this work, the validation of the model using ultrasonic water atomization was performed (Figure 7). In essence, the mean deviation of the productivity calculated by the physical model and the experimental data amounts to 0.468. The experiments showed that the traditional system produced freshwater with TDS of 0.16 g/kg in the case of using Mediterranean seawater as feedwater. In comparison, in the case of using low salinity feedwater, the freshwater resulted in a constant TDS value of 0.02 g/kg.

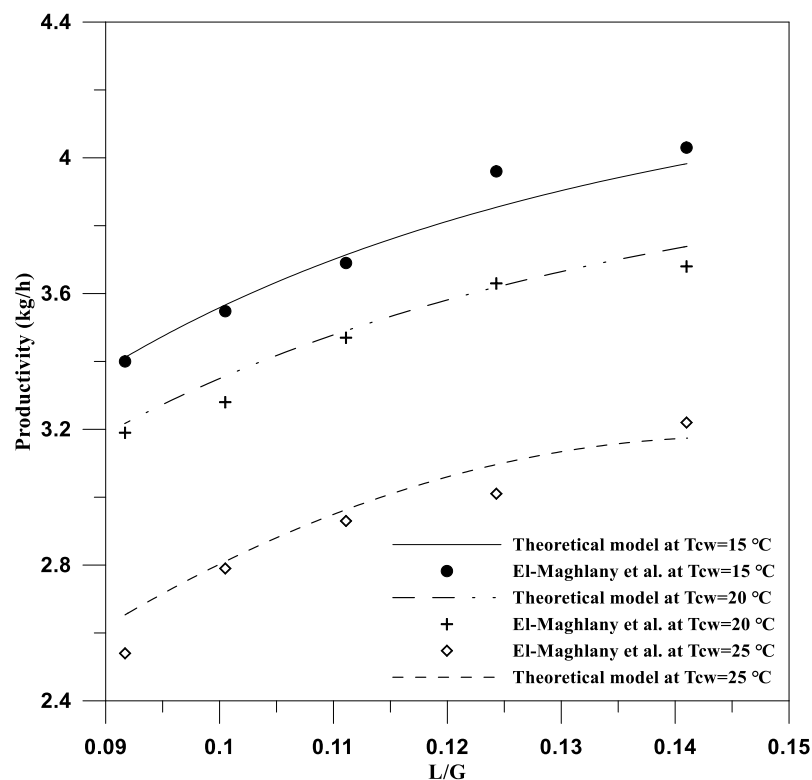


Figure 6. Productivity of the desalination unit using spraying atomization as a function of water to air mass ratios. Theoretical model results and experimental results of El Maghlany et al. [19], at different temperatures.

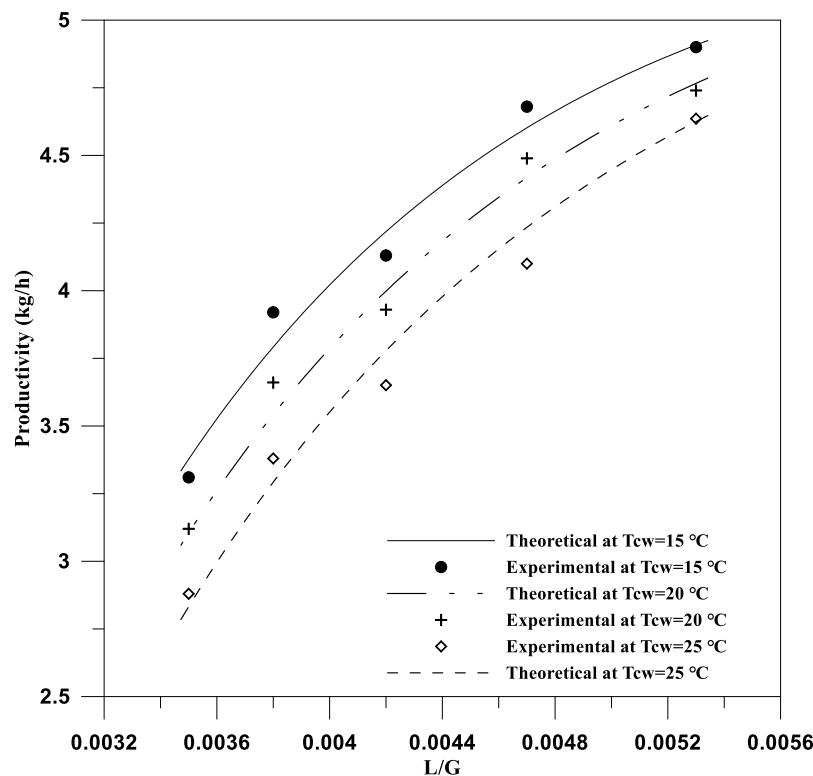


Figure 7. Productivity of the desalination unit using an ultrasonic atomizer system as a function of water to air mass ratios.

Different humidification processes (spraying atomization, ultrasonic water atomization, and hybrid atomization) are evaluated and compared in this work. Figure 8 shows the humidification effectiveness for both spraying and ultrasonic water atomization methods at the same operating conditions (dry bulb temperature of 50 °C and relative humidity of 8%). The effectiveness of the process is more significant with the ultrasonic water atomization than with the simple spraying system. The comparison between these two humidification methods should also take into account that the ultrasonic atomizer produces just 5 kg/h of vapor, whereas direct spraying produces 132 kg/h of vapor. However, the low water consumption and the high effectiveness make ultrasonic atomization a remarkable option.

Figure 9 shows a comparison between the productivity achieved by the spraying and ultrasonic humidification systems at the same ambient air inlet conditions (dry bulb temperature of 25 °C and relative humidity of 50%) at different inlet cooling water temperatures. Clearly, the productivity decreases as the temperature of the inlet cooling water increases, where the cooling load used in the dehumidification process decreases. The ultrasonic water atomizer has almost the same trend observed in its humidification effectiveness. Due to the low mass flow rate of atomized water produced compared to the amount of air flowing, the condensate tends to be near the amount of atomized water flow rate (\dot{m}_{sw}). It was observed that, for the new humidification system, the higher the capacity, the higher both productivity, and humidification effectiveness. However, to test this system, the quality of the freshwater must be checked. It has been shown that the ultrasonic water atomizer evaporates some salts with water. Figure 10 shows the amount of salt concentration in the freshwater. As the concentration of the brine in the feed water increases, the amount of salts in the freshwater increases gradually. The maximum concentration of salts in the feed water (TDS = 35, Mediterranean Sea) allowed the production freshwater for human drinking water (as reported by [2], which is a maximum of 0.5 g/kg for drinking water) not exceeding 8 g/kg, which produced output freshwater with a salt concentration of 0.35 g/kg.

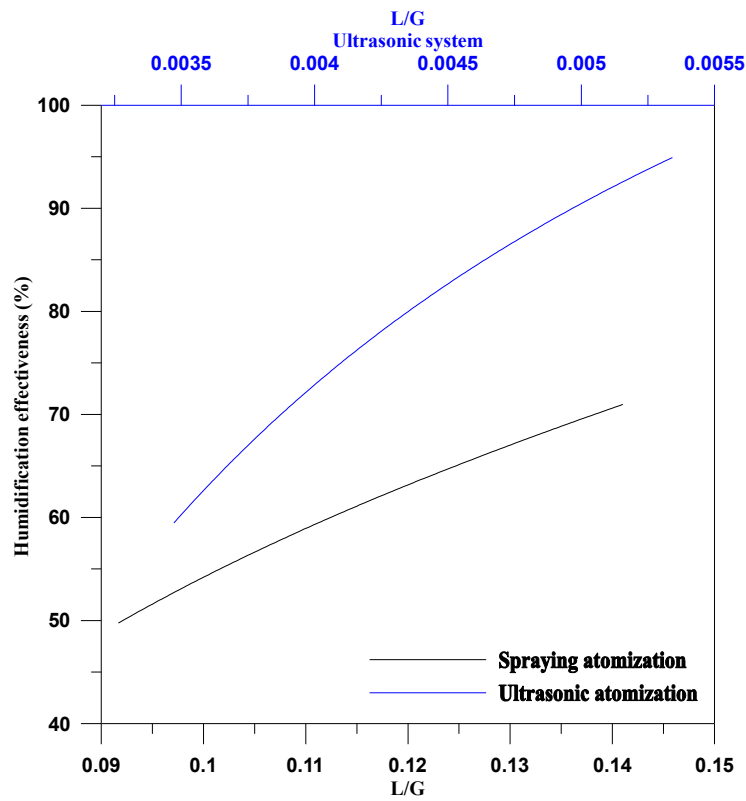


Figure 8. Effectiveness of humidification process for spraying and ultrasonic water atomizers.

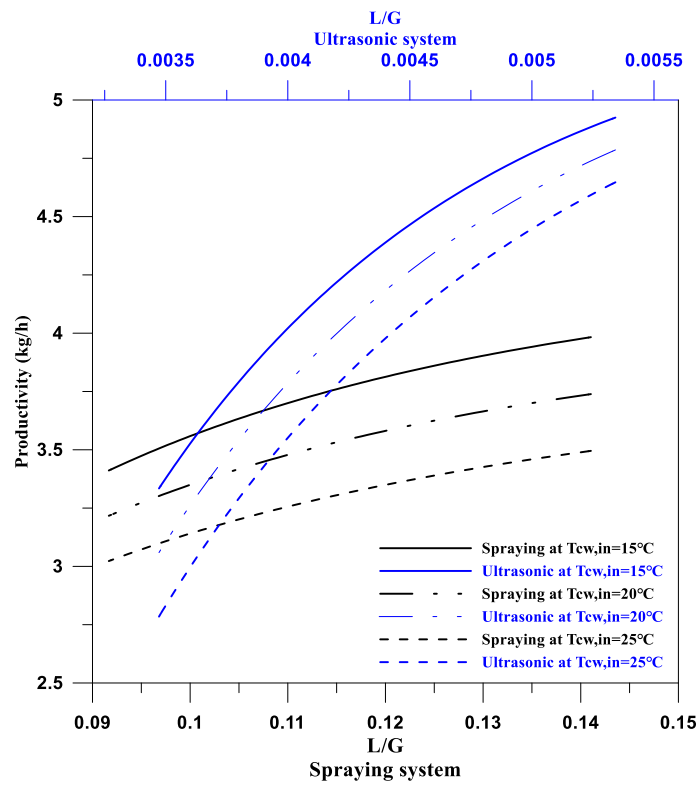


Figure 9. Productivity of traditional spraying system and ultrasonic water atomizer at different $T_{cw,in}$.

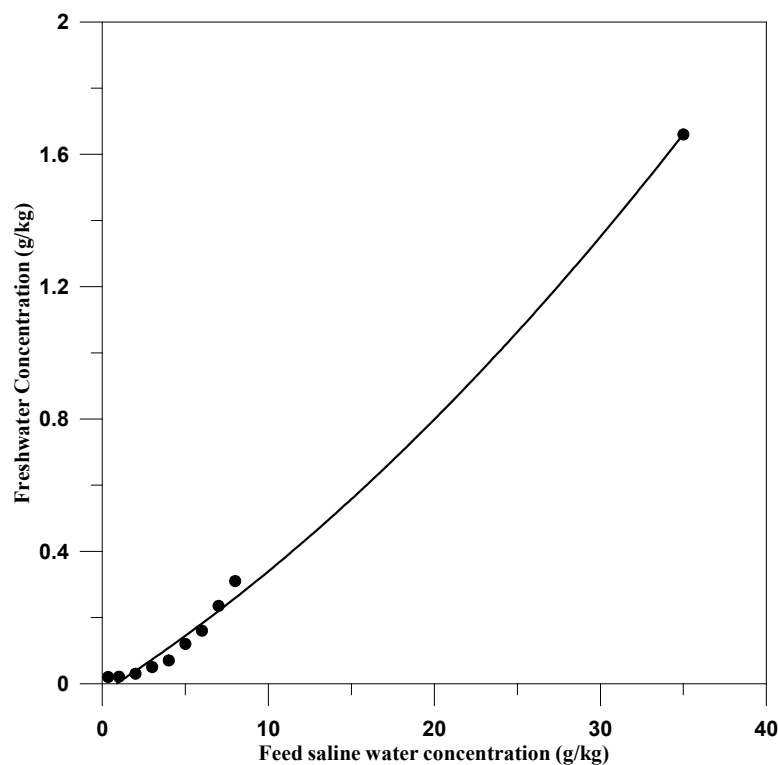


Figure 10. Productivity concentration using the ultrasonic water atomizer.

By evaluating the performance of the desalination system, the specific productivity can be considered to be an essential parameter that defines the amount of freshwater, which can be produced by consuming one unit of energy. The results calculated in this work are presented in Figure 11. The specific productivity for both humidification systems has the same trend, as seen in Figures 6 and 7. The power consumption of the ultrasonic atomizer is close to that of the saline water feed pump used in the spraying atomizer. However, the specific productivity is higher in the case of using an ultrasonic water atomizer, as it has higher productivity than the spraying system. The traditional system only appears to be more efficient for L/G ratios lower than 0.1.

Trying to improve the humidification process more and more, a hybrid humidification process is established using both spraying and ultrasonic saline water atomization, where the drain of the spraying system is used to feed the ultrasonic water atomizer. Figure 12 shows the condensate rate for the hybrid system under the same operating conditions used in the spraying and ultrasonic humidification systems (where the ambient air-dry bulb temperature is 25 °C and with 50% relative humidity). The figure shows that the difference in productivity between the different temperature operation conditions decreases with the L/G ratio (atomized saline water to air mass flow rates). This behavior does not occur in the previous humidification scenarios.

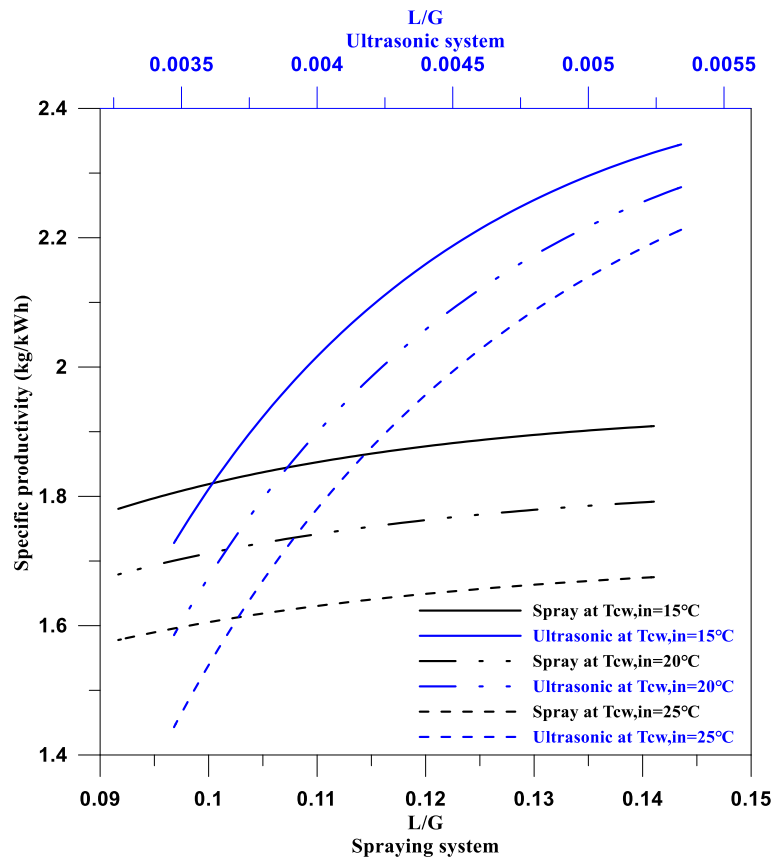


Figure 11. Specific productivity for the spraying and ultrasonic water atomizers at different $T_{cw,in}$.

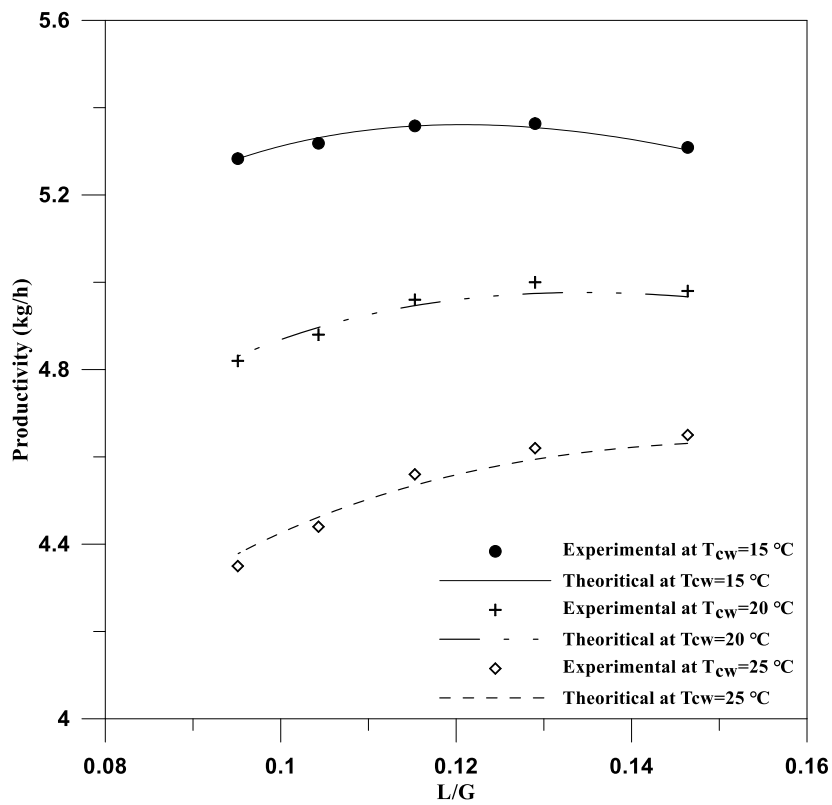


Figure 12. Productivity for the hybrid system at different inlet cooling water temperatures at the WCHE.

Figure 13 shows the effectiveness of the humidification process for each scenario at the same inlet air conditions (25 °C dry-bulb temperature and 50% relative humidity). The hybrid system presents higher effectiveness due to its higher requirement of atomized water.

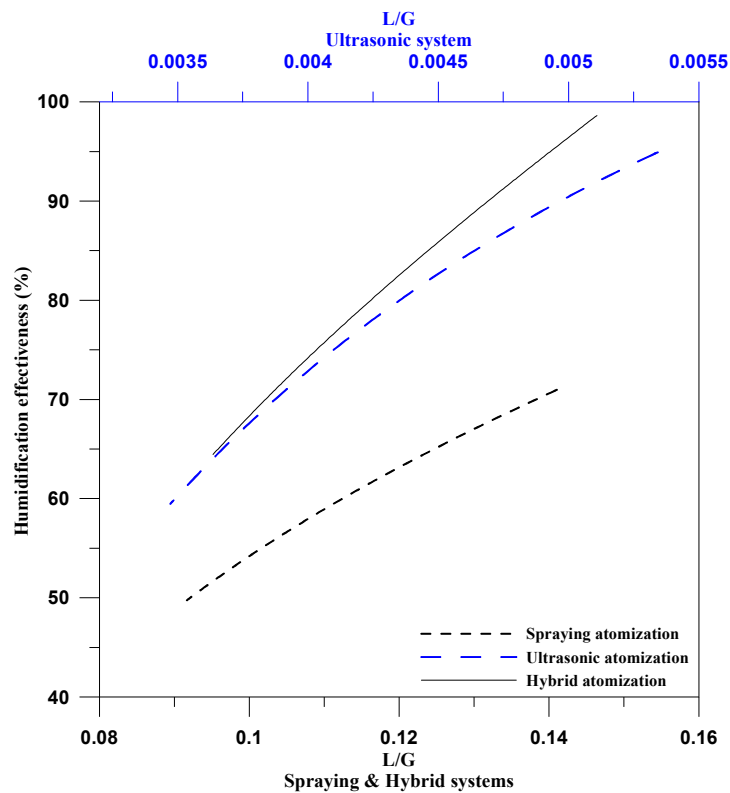


Figure 13. Comparison of the three humidification systems.

Figure 14 compares the productivity of each humidification system showing the condensate rate at different inlet cooling water temperatures to the WCHE. Obviously, productivity decreases as the inlet cooling water temperature decreases. The hybrid system has higher productivity than the other systems because its requirements of atomized saline water are also higher. However, in the hybrid system, the change in the condensate rate with the saline water to the airflow rate ratio is so small. In this operation (hybrid system), the air is close to being saturated, while the cooling capacity of both WCHE and heat pump evaporator could not extract more freshwater from this saturated air. This scenario can be demonstrated from the relation between productivity and the humidification effectiveness of the hybrid system. As humidification effectiveness increases, productivity also does. However, at L/G of 0.12, the productivity begins to decrease as the amount of saline water increases due to its low cooling capacity.

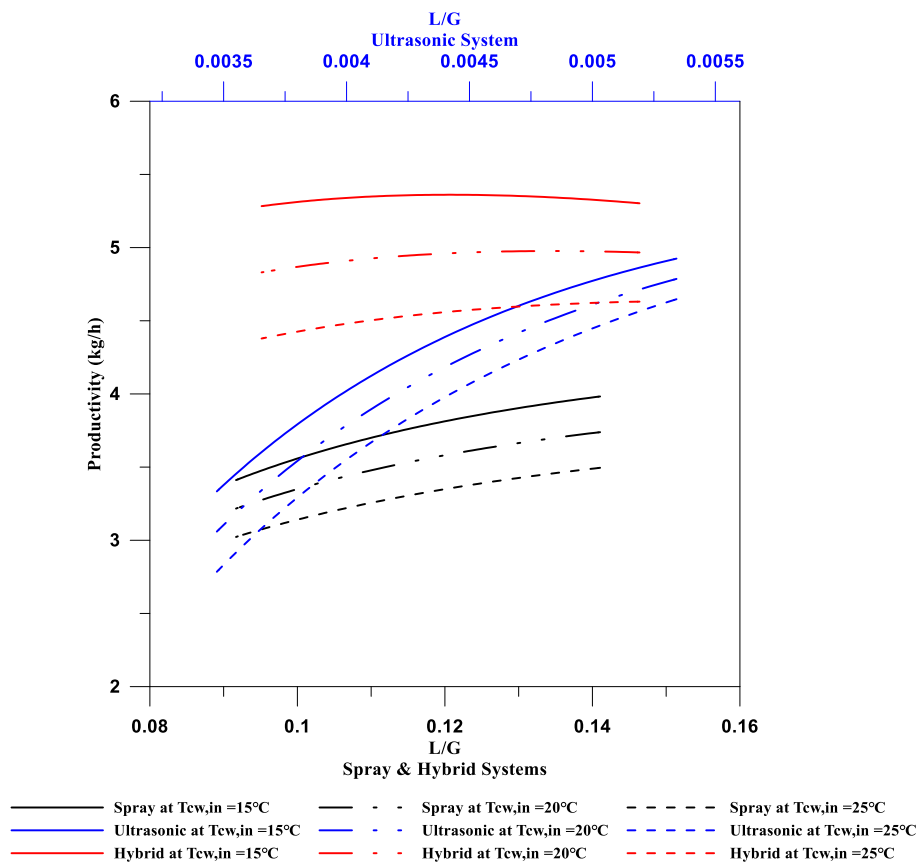


Figure 14. Productivity of the three systems at different $T_{cw, in}$.

Using the spraying and ultrasonic water atomizers, the specific productivity increases as the amount of atomized water increases. However, in the case of the hybrid system, the specific productivity has a different trend: Figure 15 shows that when the amount of atomized water increases, the specific productivity slightly decreases. According to Figure 12, the condensate rate for the hybrid system has a small variation over the ratios of saline water and airflows. In addition to that, the power consumption decreases as the mass flow rate of air also does due to productivity reduction. As mentioned in the previous section: at low temperatures (15 and 20 °C), the lower the L/G ratio, the lower the heating load on the compressor and, the higher the L/G ratio, the lower the specific productivity. On the other hand, as the ratio decreases, where the heating load on the compressor drops, the specific productivity is reduced. In the other two systems, the specific productivity increases as the condensate rate also does. There is a huge difference in the condensate rate especially between the traditional atomization and hybrid systems. The trend of the specific productivity is the same for the three cases of humidification process at different inlet cooling water temperatures to the WCHE, and, obviously, the higher the temperature, the lower the specific productivity.

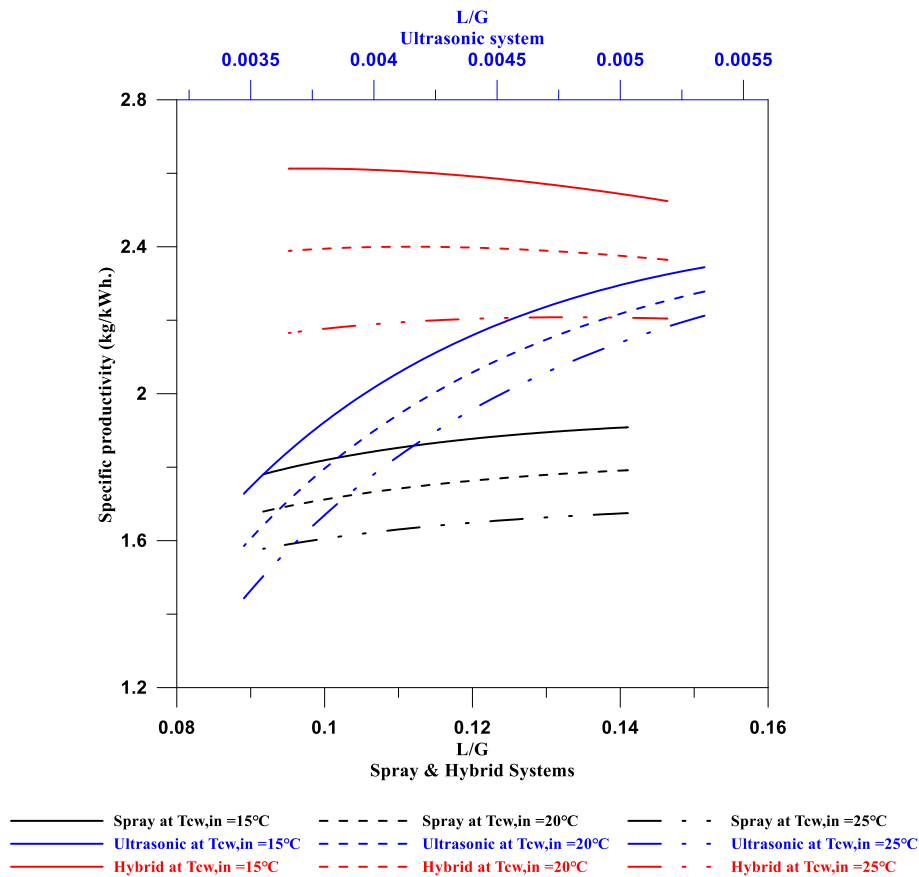


Figure 15. Specific productivity of the three systems at different $T_{cw,in}$.

6. Cost Analysis

In this section, a cost analysis is performed on the proposed desalination systems in order to evaluate the desalination systems (spraying, ultrasonic, and hybrid atomization in the humidification process) from an economic point of view.

The costs of the various components used in the proposed humidification–dehumidification (HDH) desalination unit, based on the Egyptian market prices in 2019, are given in Table 2. The capital cost estimated for the HDH desalination system amounts to \$535. To obtain the cost of the freshwater produced by these systems, other parameters must be taken into consideration: assuming installation costs to be 10% of the capital cost; expected lifetime (N), 10 years; inflation rate (dd), 8.65%; interest rates (i), 11.9% (based on 2020 Egyptian economic statistics). In addition to this, a yearly maintenance cost (M/yr) of 5% of the capital cost has been considered for the following components: the centrifugal fan, the control panel, the water sprayers, the ultrasonic atomizer, and the feed pumps. Therefore, the PW of the maintenance cost (C_{MPW}) can be calculated using Equation (42) to be \$99.4, \$145.9, and \$146.35 for the spraying, ultrasonic, and hybrid water atomizers, respectively, using the maintenance cost per year (M/yr) and the lifetime of the system ($N = 10$ years).

$$C_{MPW} = \left(\frac{M}{yr}\right) \times \left[\frac{1+i}{1+dd}\right] \times \left\{ \frac{1 - \left(\frac{1+i}{1+dd}\right)^N}{1 - \left(\frac{1+i}{1+dd}\right)} \right\} \tag{42}$$

Table 2. Estimated capital cost for HDH components (2018 Egyptian market).

Components	Capital Cost (\$)	Components	Capital Cost (\$)
Centrifugal fan	30	Ultrasonic atomizer	110
Flexible duct	2	Feed pump I	12
Compressor	151	Feed pump II	12
Heat pump condenser	30	Heat pump evaporator	25
Water eliminator	20	Piping	2
Control panel	25	Steel construction stands	85
Two water sprayers	1	Insulated ducts	30
Total capital cost		\$535	

The running cost ($C_{running}$) was calculated taking into account that this unit is powered by electricity, and assuming an average cost of \$0.048 per kWh of electric energy, where the electric energy consumption for the desalination unit at different operating conditions was considered. The main variation in electric power consumption comes from changes in the air mass flow rate, which consequently affect fan power. In addition to this, the variation in air mass flow rate that passes through the heat pump condenser affects the heat pump compressor power consumption (based on the experiments carried out).

Calculating the life cycle cost analysis of the desalination system using Equation (43):

$$LCC = C_{capital} + C_{installation} + C_{MPW} + C_{running} \tag{43}$$

Finally, the total annual cost (TAC), which is a function of the capital, running, and maintenance costs, was calculated for each system using Equation (44). The values of TAC differ, as mentioned before, due to the difference in electric power consumption in each operating condition (due to the change in air mass flow rate and the cooling capacity of the heat pump), as presented in Table 3. To get the cost of the freshwater produced using Equation (45), the TAC is divided by the freshwater produced per year. Therefore, the cost analysis showed that the cost per kilogram of freshwater varies from \$0.0311 to \$0.0328 for the spraying, \$0.0251 to \$0.0306 in the case of using the ultrasonic, and \$0.0250 to \$0.0233 for the hybrid system.

$$TAC = LCC \times \left\{ \frac{1 - \left(\frac{1+i}{1+dd} \right)^N}{1 - \left(\frac{1+i}{1+dd} \right)} \right\} \tag{44}$$

$$Unit\ cost\ of\ freshwater = \frac{TAC}{8760 \times m_{FW}} \tag{45}$$

Table 3. Total annual cost and electric energy consumption for the three humidification systems in different operations.

Humidification Systems Used	Electric Energy Consumption/Year (E_L) vs. the Total Annual Cost for Each Humidification System (TAC)									
	kWh/yr	(LE/yr)	kWh/yr	(LE/yr)	kWh/yr	(LE/yr)	kWh/yr	(LE/yr)	kWh/yr	(LE/yr)
Spraying	18,279.4	1064.03	18,158.1	1057.40	17,942.2	1045.61	17,294.7	1010.24	16,782	982.25
Ultrasonic	18,402.1	1086.14	18,280.7	1079.51	18,064.8	1067.72	17,417.3	1032.36	16,904.7	1004.36
Hybrid	19,751.2	1162.25	19,629.7	1155.62	19,412.1	1143.84	18,766.4	1108.47	18,253.7	1080.48

According to the cost analysis presented for the three humidification systems used, the hybrid system has the least cost per kilogram of freshwater. In comparing the freshwater cost to other desalination systems such as seawater reverse osmosis (SWRO), the cost is high [6]. However, although the cost of this technology is still well above other more cost-effective technologies, such as seawater reverse osmosis, it can be considered a viable alternative in remote and arid areas, where there is not an adequate electric power supply to operate reverse osmosis. Other benefits for its affordable

installation in dry and isolating regions include: (a) simple operation, (b) low maintenance requirements (c) low-temperature thermal energy demand, which can be easily obtained from a renewable source.

7. Conclusions

In this study, a water desalination system based on the HDH process using a heat pump was experimentally and theoretically investigated. A new humidification process (ultrasonic water atomization) was used in the application of water desalination systems. In addition to this, a hybrid humidification system was established. The results showed that the ultrasonic water atomizer provided higher humidification effectiveness than the traditional humidification process (spraying atomization). Moreover, the power consumption of the new system was nearly the same as the power consumption of the spraying atomization system. However, the ultrasonic water atomizer is limited to feedwater salinity of over 8 g/kg, while the spraying system is capable of dealing with all types of feed water at different salinities. The maximum productivity achieved by the desalination unit was 4.9 kg/h in the case of using an ultrasonic water atomizer, while in the case of using the hybrid system, it was 5.36 kg/h. A cost analysis for the three systems (spraying, ultrasonic, and hybrid atomization systems) was performed, resulting in minimum costs for one kilogram of freshwater of \$0.0311, \$0.0251, and \$0.0233, respectively.

Author Contributions: A.E.T. conceived and planned the experiments, carried out the experiments, and performed the analytic calculations and performed the numerical simulations. A.M.B.-M. and M.J.S.-L. discussed the results and contributed to the final manuscript. A.M.B.-M., A.M.E., and M.J.S.-L. supervised the paper. All authors have read and agreed to the published version of the manuscript.

Funding: This research received no external funding.

Conflicts of Interest: The authors declare that they have no known competing financial interests or personal relationships that could have appeared to influence the work reported in this paper.

Nomenclature

a	Air
A	Surface area (m ²)
A_{in}	Inlet cross-sectional area (m ²)
A_{out}	Outlet cross-sectional area (m ²)
A_{fin}	Fin surface area (m ²)
C	Condenser
$c_{p,sw}$	Saline water specific heat capacity (kJ/kg.K)
$c_{p,a}$	Dry air specific heat capacity (kJ/kg.K)
$c_{p,v}$	Water vapor specific heat capacity (kJ/kg.K)
CW	Cooling water
d	Diameter (m)
dd	Inflation rate (%)
E	Evaporator
E_L	Electric energy consumption (kWh)
h	Specific enthalpy (kJ/kg)
H	Humidifier
h_{fg}	Latent heat of vaporization (kJ/kg)
I	Electric current (A)
i	Interest rate (%)
k	Thermal conductivity (W/m.K)
l	Length (m)
L	Losses

\dot{m}_a	Air mass flow rate (kg/s)
\dot{m}_R	Refrigerant mass flow rate (kg/s)
\dot{m}_{FW}	Condensate mass flow rate (kg/s)
\dot{m}_{vap}	Ultrasonic water vapor flow rate (kg/s)
P	Perimeter (m)
Pr	Prandtl number
r	Radius (m)
R	Refrigerant
Re	Reynolds number
V	Voltage (V)
\dot{W}_{elec}	Electric power consumption

Abbreviations

CAOW-AH	Closed-air, Open-water, and air heated
CAOW-WH	Closed-air, Open-water, and water heated
Conv	Heat transfer by convection
HDH	Humidification-Dehumidification
IPCC	Intergovernmental Panel on Climate Change
L/G	Atomized water to airflow mass ratio
LCC	Life cycle cost
OAOW-WH	Open-air, Open-water, and water heated
TDS	Total Dissolved Salts
TAC	Total Annual Cost
WCHE	Water Cooled Heat Exchanger

Greek Symbols

ε_h	Humidification efficiency
ε_{deh}	Dehumidification efficiency
ω	Humidity ratio (kg _w /kg _{air})
η	Efficiency

References

1. Mayere, M. Solar Power Desalination. Ph.D. Thesis, University of Nottingham, Nottingham, UK, 2011.
2. UNESCO World Water Assessment Programme (WWAP). The United Nations World Water Development Report. 2019. Available online: <https://www.unwater.org/publications/world-water-development-report-2019/> (accessed on 26 March 2020).
3. Al-Karaghoul, A.; Kazmerski, L.L. Energy consumption and water production cost of conventional and renewable-energy-powered desalination processes. *Renew. Sustain. Energy Rev.* **2013**, *24*, 343–356. [[CrossRef](#)]
4. El-Agouz, S.A.; Sathyamurthy, R.; Manokar, A.M. Improvement of humidification–dehumidification desalination unit using a desiccant wheel. *Chem. Eng. Res. Des.* **2018**, *131*, 104–116. [[CrossRef](#)]
5. Hou, S.; Zhang, H. A hybrid solar desalination process of the multi-effect humidification dehumidification and basin-type unit. *Desalination* **2008**, *220*, 552–557. [[CrossRef](#)]
6. Muthusamy, C.; Srithar, K. Energy saving potential in humidification-dehumidification desalination system. *Energy* **2017**, *118*, 729–741. [[CrossRef](#)]
7. Deniz, E.; Çınar, S. Energy, exergy, economic and environmental (4E) analysis of a solar desalination system with humidification-dehumidification. *Energy Convers. Manag.* **2016**, *126*, 12–19. [[CrossRef](#)]
8. Santosh, R.; Arunkumar, T.; Velraj, R.; Kumaresan, G. Technological advancements in solar energy driven humidification-dehumidification desalination systems—A review. *J. Clean. Prod.* **2018**, *207*, 826–845. [[CrossRef](#)]
9. Zamen, M.; Soufari, S.; Vahdat, S.A.; Amidpour, M.; Zeinali, M.; Izanloo, H.; Aghababaie, H. Experimental investigation of a two-stage solar humidification–dehumidification desalination process. *Desalination* **2014**, *332*, 1–6. [[CrossRef](#)]
10. Kabeel, A.; El-Said, E.M. A hybrid solar desalination system of air humidification, dehumidification and water flashing evaporation: Part II. Experimental investigation. *Desalination* **2014**, *341*, 50–60. [[CrossRef](#)]

11. Hamed, M.H.; Kabeel, A.; Omara, Z.; Sharshir, S. Mathematical and experimental investigation of a solar humidification–dehumidification desalination unit. *Desalination* **2015**, *358*, 9–17. [[CrossRef](#)]
12. Gao, P.; Zhang, L.; Zhang, H. Performance analysis of a new type desalination unit of heat pump with humidification and dehumidification. *Desalination* **2008**, *220*, 531–537. [[CrossRef](#)]
13. Yuan, G.; Zhang, L.; Zhang, H. Experimental research of an integrative unit for air-conditioning and desalination. *Desalination* **2005**, *182*, 511–516. [[CrossRef](#)]
14. Xu, L.; Chen, Y.-P.; Wu, P.-H.; Huang, B.-J. Humidification–Dehumidification (HDH) Desalination System with Air-Cooling Condenser and Cellulose Evaporative Pad. *Water* **2020**, *12*, 142. [[CrossRef](#)]
15. Yanniotis, S.; Xerodemas, K. Air humidification for seawater desalination. *Desalination* **2003**, *158*, 313–319. [[CrossRef](#)]
16. Kang, H.; Yang, Y.; Chang, Z.; Zheng, H.; Duan, Z. Performance of a two-stage multi-effect desalination system based on humidification–dehumidification process. *Desalination* **2014**, *344*, 339–349. [[CrossRef](#)]
17. Hawlader, M.; Dey, P.K.; Diab, S.; Chung, C.Y. Solar assisted heat pump desalination system. *Desalination* **2004**, *168*, 49–54. [[CrossRef](#)]
18. Hegazy, A.H.; Teamah, M.A.; Hanafy, A.A.; El-Maghlany, W.M. Experimental study of a water desalination system based on humidification–dehumidification process using a heat pump. *Energy* **2015**. [[CrossRef](#)]
19. El-Maghlany, W.M.; Tourab, A.E.; Hegazy, A.H.; Teamah, M.A.; Hanafy, A.A. Experimental study on productivity intensification of HDH desalination unit utilizing two-stage dehumidification. *Desalin. Water Treat.* **2018**, *107*, 28–40. [[CrossRef](#)]
20. Elminshawy, N.; Siddiqui, F.R.; Addas, M.F. Experimental and analytical study on productivity augmentation of a novel solar humidification–dehumidification (HDH) system. *Desalination* **2015**, *365*, 36–45. [[CrossRef](#)]
21. Gang, W.; Zheng, H.; Kang, H.; Yang, Y.; Cheng, P.; Chang, Z. Experimental investigation of a multi-effect isothermal heat with tandem solar desalination system based on humidification–dehumidification processes. *Desalination* **2016**, *378*, 100–107. [[CrossRef](#)]
22. El-Agouz, S.; Abugderah, M. Experimental analysis of humidification process by air passing through seawater. *Energy Convers. Manag.* **2008**, *49*, 3698–3703. [[CrossRef](#)]
23. Ghazal, M.; Atikol, U.; Egelioglu, F. An experimental study of a solar humidifier for HDD systems. *Energy Convers. Manag.* **2014**, *82*, 250–258. [[CrossRef](#)]
24. Deepu, P.; Peng, C.; Moghaddam, S. Dynamics of ultrasonic atomization of droplets. *Exp. Fluid Sci.* **2018**, *92*, 243–247. [[CrossRef](#)]
25. Zhang, L.; Dong, H.; Wang, X. Temperature Response in the Process of Ultrasonic Seawater Desalination. In *Proceedings of the Asia-Pacific Power and Energy Engineering Conference*, Wuhan, China, 25–28 March 2011; pp. 1–4.
26. Kline, S.; McClintock, F. Describing uncertainties in single sample experiments. *Mech. Eng.* **1953**, *75*, 3–8.
27. Cengel, Y. *Heat and Mass Transfer*, 2nd ed.; McGraw-Hill: Boston, MA, USA, 2014; p. 694.
28. Picinardi, A. Cogeneration of Cooling Energy and Freshwater. Ph.D. Thesis, University of Bergamo, Bergamo, Italy, 2011.
29. Sharqawy, M.H.; Antar, M.A.; Zubair, S.M.; Elbashir, A.M. Optimum thermal design of humidification dehumidification desalination systems. *Desalination* **2014**, *349*, 10–21. [[CrossRef](#)]

